Neural Network-Based Inverse Design of Nonlinear Phononic Crystals

KUNQI HUANG[1,2], YUANYUAN LI[1,2], YUN LAI[1,2], AND XIAOZHOU LIU[1,2,3]

[1]Key Laboratory of Modern Acoustics, Institute of Acoustics, Nanjing University, Nanjing 210093, China
[2]School of Physics, Collaborative Innovation Center of Advanced Microstructures, Nanjing University, Nanjing 210093, China
[3]State Key Laboratory of Acoustics, Institute of Acoustics, Chinese Academy of Sciences, Beijing 100190, China

CORRESPONDING AUTHORS: Y. LAI (laiyun@nju.edu.cn) and X. LIU (xzliu@nju.edu.cn)

ABSTRACT Phononic crystals are artificial periodic structural composites. With the introduction of nonlinearity, nonlinear phononic crystals(NPCs) have shown some novel properties beyond their linear counterparts and thus attracted significant interest recently. Among these novel properties, the second harmonic characteristics have potential applications in the fields of acoustic frequency conversion, non-reciprocal propagation, and nondestructive testing. Therefore, how to accurately manipulate the second harmonic band structure is a main challenge for the design of NPCs. Traditional design methods are based on parametric analysis and continuous trials, leading to low design efficiency and poor performance. Here, we construct the convolutional neural networks(CNNs) and the generalized regression neural networks(GRNNs) to inversely design the physical and geometric parameters of NPCs using the information of harmonic transmission curves. The results show that the inverse design method based on neural networks is effective in designing the NPCs. In addition, the CNNs have better prediction accuracy while the GRNNs have a shorter training time. These methods also can be applied to the design of higher-order harmonic band structures. This work confirms the feasibility of neural networks for designing the NPCs efficiently according to target harmonic band structures and provides a useful reference for inverse design of metamaterials.

INDEX TERMS Neural network, nonlinearity, phononic crystal, inverse design.

I. INTRODUCTION

PHONONIC crystals are composite materials with a periodic structure. The dispersion relations of phononic crystals usually exhibit unique bandgap structures due to wave scattering or local resonance of the periodic structure [1]. In recent years, by introducing nonlinearity into phononic crystal systems, novel nonlinear properties in the wave propagation that cannot be realized by linear systems have been achieved. For example, nonlinear systems can exhibit novel wave responses, such as isolated wave propagation, higher harmonic generation, and non-reciprocal wave propagation, which have important applications [2], [3], [4], [5]. As the wave propagates through the nonlinear phononic crystals(NPCs), fundamental wave energy is converted into higher frequency waves, and this conversion is called harmonic generation. Although second harmonic generation is very common in NPCs, designing

the NPCs with the ideal harmonic band structure is still a challenging problem due to material inhomogeneities and computational complexity [5], [6], [7].

In the last decades, phononic crystals have been designed by tuning the physical properties of materials and acoustic parameters to match specific dispersion characteristics [8], [9]. This traditional method requires empirical and experimental support, and the design process is complex, consuming a lot of time and computer memory. In recent years, artificial intelligence technology has developed rapidly. Neural networks, as an important part of artificial intelligence technology, are widely used in various fields such as computer vision, speech recognition, and natural language processing. Compared with traditional genetic algorithms, neural networks can find the global optimal solution much faster in the search space using large training data. Neural networks are not only able to learn and represent complex nonlinear

mapping relationships, but also can be accelerated by parallel computing. Therefore, it has obvious superiority in dealing with complex, nonlinear problems. Inspired by artificial intelligence technology, the application of neural networks in metamaterial design has also started to receive attention [10], [11], [12], [13]. For example, Peurifoy et al. trained neural networks to approximate light scattering from multilayer nanoparticles [14]. Finol et al. used deep convolutional neural networks and conventional densely connected neural networks to predict the eigenvalues of phononic crystals and concluded that deep convolutional neural networks outperformed conventional densely connected neural networks [15]. Ahmed et al. designed a broadband acoustic cloak based on a probabilistic deep-learning model [16]. Liu et al. implemented the inverse design of an acoustic ultra-material plate by constructing the deep-learning neural networks model using the desired bandgap center frequency and bandwidth as inputs [17]. Gurbuz et al. proposed a method for designing acoustic metamaterials based on generative adversarial neural networks, which successfully achieved the inverse design of structural metamaterials [18]. Liu et al. used supervised learning neural networks and unsupervised learning neural networks for the design of phononic crystals [19]. He et al. applied the reinforcement learning algorithm and deep tandem neural network to complete the inverse design of elastic phononic beams [20].

Although previous studies have illustrated the feasibility of applying neural networks to the inverse design of phononic crystals, however, they are all limited in linear metamaterials, and most of them use dispersion characteristic analytical solutions to construct the dataset. Unlike previous studies, we explore the application of neural networks in the design of NPCs for the first time. On the one hand, the dispersion characteristics of the second harmonic are difficult to obtain by analytical solutions, so the use of transmission characteristics to inversely design NPCs is necessary. On the other hand, phononic crystals have finite periods in practical engineering. Therefore, it is more accurate to use the transmission characteristics to evaluate the band structure than to use the dispersion characteristics.

The purpose of this paper is to use neural networks for designing NPCs with the specific second harmonic band structure. The neural networks method not only can reduce the computational cost but also can keep the designed NPCs' transmission characteristics highly consistent with the target transmission characteristics. First, for generating the data set, we calculate the transmission curves of the second harmonic in a one-dimensional two-phase NPC using the finite element method(FEM). Then, we introduce the principles and basic structures of two neural network models named the convolutional neural networks(CNNs) and the generalized regression neural networks(GRNNs), and illustrate the NPC inverse design process. Finally, three cases are investigated, i.e., two-parameter, three-parameter, and four-parameter predictions, and the performance of the two neural networks is tested. This work provides an effective method for designing NPCs
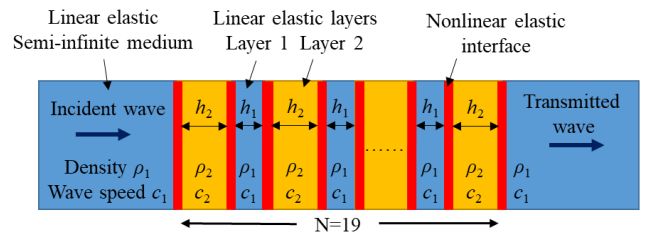

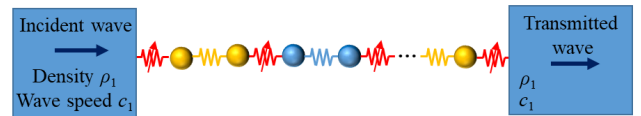FIGURE 1. A multilayered NPC model with nonlinear interfaces.

FIGURE 2. A NPC discretization model (finite waveguide is approximated as two masses coupled with a linear spring, and the interface interaction is approximated as a nonlinear spring).

with the specific harmonic band structure, demonstrating new ideas for better implementation of frequency conversion devices or acoustically nonreciprocal transmission.

II. THEORETICAL ANALYSIS
A. NPC MODEL
The purpose of NPC inverse design is to input the band structure of the second harmonic transmission curve and then output the corresponding physical and geometric parameters. We can use the powerful nonlinear fitting function of the neural network to realize the fast design of the second harmonic band structure.

The model that generates the dataset is shown in Fig. 1, which considers the longitudinal wave propagation in the layered direction of the one-dimensional multilayer structure. The structure consists of two different types of N alternating linear elastic layers, which are layer 1 (density ρ_1, wave velocity c_1, thickness h_1) and layer 2 (density ρ_2, wave velocity c_2, thickness h_2). They are embedded between two linearly elastic semi-infinite media with the same properties as the layer 1 media. All these media can be regarded as interconnected at the interface through N+1 nonlinear elastic interfaces. To ensure that the different linear elastic layers are connected alternately, we set N to an odd number.

The wave propagation phenomenon in this nonlinear system is difficult to solve exactly in analytical form, so here we establish a discrete mass-spring model of this structure (as in Fig. 2) for analysis. This is a classical method that can easily realize the numerical analysis of this nonlinear structure [21], [22], [23], [24], [25], [26].

The motion equation of this structure is shown as (1).

With initial incentive:

$$u_{inc}(x - c_1 t) = A \cos\left(\omega c_1^{-1}(x - c_1 t)\right). \quad (1)$$

Here u is the mass displacement, A is the initial amplitude, ω is the angular frequency of the wave, and t is the time.

If the nth layer is the linear elastic layer i ($i = 1$ or 2), its corresponding motion equation is:

$$\frac{\rho_i h_i}{2}\ddot{u}_{n,1} + \frac{2\rho_i c_i^2}{h_i}\left(u_{n,1} - u_{n,2}\right) = -f\left(u_{n,1} - u_{n-1,2}\right), \quad (2)$$

$$\frac{\rho_i h_i}{2}\ddot{u}_{n,2} - \frac{2\rho_i c_i^2}{h_i}\left(u_{n,1} - u_{n,2}\right) = f\left(u_{n+1,1} - u_{n,2}\right). \quad (3)$$

Here $\ddot{u}_{n,1}$ and $\ddot{u}_{n,2}$ denote the displacement of the first and the second mass of the nth layer. f denotes the nonlinear interface interaction force.

In the case of spring-type interfaces with weak quadratic nonlinearity, the nonlinear interface equation is:

$$f\left(\Delta u\right) = K\left(1 - \beta\Delta u\right)\Delta u. \quad (4)$$

Here K is the interface linear stiffness, β is a positive parameter representing the interface nonlinearity and Δu represents the relative displacement at the interface.

The boundary conditions of the model are:

$$\rho_1 c_1 \dot{u}_0 = K\left(u_{1,1} - u_0\right) - \beta K^2\left(u_{1,1} - u_0\right)^2 \\ - 2\rho_1 c_1^2 u_{inc}(-c_1 t), \quad (5)$$

$$\rho_1 c_1 \dot{u}_{N+1} = -K\left(u_{N+1} - u_{N,2}\right) + \beta K^2\left(u_{N+1} - u_{N,2}\right)^2. \quad (6)$$

Here u_0 is the displacement at the end of the first semi-infinite medium, which is at $x = 0$. And u_{N+1} is the displacement at the beginning of the second semi-infinite medium, which is at $x = \frac{h_1(N-1)+h_2(N+1)}{2}$. Rearranging the above equation yields:

$$\dot{u}_0 = \frac{K}{\rho_1 c_1}\left(u_{1,1} - u_0\right) - \frac{\beta K^2}{\rho_1 c_1}\left(u_{1,1} - u_0\right)^2 - 2A\omega\sin(\omega t), \quad (7)$$

$$\ddot{u}_{n,1} = -\frac{4c_i^2}{h_i^2}\left(u_{n,1} - u_{n,2}\right) - \frac{2K}{\rho_i h_i}\left(u_{n,1} - u_{n-1,2}\right) \\ + \frac{2\beta K^2}{\rho_i h_i}\left(u_{n,1} - u_{n-1,2}\right)^2, \quad (8)$$

$$\ddot{u}_{n,2} = \frac{4c_i^2}{h_i^2}\left(u_{n,1} - u_{n,2}\right) + \frac{2K}{\rho_i h_i}\left(u_{n+1,1} - u_{n,2}\right) \\ - \frac{2\beta K^2}{\rho_i h_i}\left(u_{n+1,1} - u_{n,2}\right)^2, \quad (9)$$

$$\dot{u}_{N+1} = -\frac{K}{\rho_1 c_1}\left(u_{N+1} - u_{N,2}\right) + \frac{\beta K^2}{\rho_1 c_1}\left(u_{N+1} - u_{N,2}\right)^2. \quad (10)$$

The goal is to use neural networks to find features in the dataset and predict material parameters for the NPC with the target second harmonic passband. We use the ODE45 finite element method(FEM) to solve (7)-(10) for displacement's numerical solutions. After obtaining the displacement signal at the end of the waveguide, we calculate the second harmonic amplitude $A_{2\omega}$ by processing the steady-state displacement signal using the fast Fourier transform. For better feature extraction, we obtain the transmission spectrum curve of

TABLE 1. Model initial parameters.

$\rho_1 = 2700\text{kg/m}^3$	$c_1 = 3000 m/s$	$h_1 = 0.003\text{m}$
$K_{max}=6 \times 10^{13}\text{N/m}$	$\beta = 5 \times 10^3$	$A = 5\mu m$

the second harmonic by calculating the transmittance based on (11).

$$T = 10\log\left|\frac{A_{2\omega}}{A}\right|. \quad (11)$$

B. THE DATA SET

For the longitudinal wave propagation of this model, the material density ratio ζ, wave velocity ratio η, and normalized interface linear stiffness $\overline{K}$ are the main physical parameters affecting the second harmonic behavior, and the material thickness ratio Λ is also an important factor. ζ, η, $\overline{K}$, Λ are defined as (12). K_{max} is the largest value in the K data set. Since the β mainly affects the second harmonic magnitude, but not its band structure distribution, it is not included as an output parameter of the neural network in this paper. Therefore, in the inverse design of the NPC, the second harmonic transmission curve can be used as the neural network input. The physical parameters ζ, η, K_{max} and the geometric parameter Λ can be used as the neural network output.

$$\zeta = \frac{\rho_1}{\rho_2}, \eta = \frac{c_1}{c_2}, \overline{K} = \frac{K}{K_{max}}, \Lambda = \frac{h_1}{h_2}. \quad (12)$$

In addition, we need to set the initial parameters of the model as shown in Table 1.

The data set consists of the training set and the testing set, and the data in the training set and the testing set are different. Then we consider three cases. For the first case, the training set A and the testing set A consist of 80 and 20 sets of data, respectively, where $\Lambda = 0.81$ and $\overline{K} = 0.63$ unchanged and the values of ζ and η range from 0.50 to 1.00 and 0.60 to 1.10; for the second case, the training set B and the testing set B consist of 800 and 200 sets of data, respectively, where $\Lambda = 0.81$ remains unchanged and the values of ζ, η and $\overline{K}$ are in the ranges 0.50-1.00, 0.60-1.10 and 0.17-1.00; for the third case, the training set C and the testing set C consist of 8000 and 2000 sets of data, where ζ, η, $\overline{K}$ and Λ take values in the ranges 0.50-1.00, 0.60-1.10, 0.17-1.00 and 0.65-1.00, respectively. In order to make the first passband and stopband of the transmission curve fall in the range of 0 to 1 MHz as much as possible, physical parameters in these range are used. The specific values of ζ, η, $\overline{K}$ and Λ are shown in Table 2.

III. NEURAL NETWORK-BASED INVERSE DESIGN METHOD

After the second harmonic transmission curve of the NPC is obtained using the FEM, further features need to be extracted to serve as training data available for the neural network. The detailed steps are as follows. Firstly, we determine the frequency range of the second harmonic to be designed and

TABLE 2. The specific values of ζ, η, $\overline{K}$ and Λ.

ζ	η	$\overline{K}$	Λ
0.50	0.60	0.17	0.65
0.56	0.66	0.26	0.69
0.61	0.71	0.35	0.73
0.67	0.77	0.44	0.77
0.72	0.82	0.54	0.81
0.78	0.88	0.63	0.84
0.83	0.93	0.72	0.88
0.89	0.99	0.81	0.92
0.94	1.04	0.91	0.96
1.00	1.10	1.00	1.00

FIGURE 3. CNN model graph.

divide the entire frequency range into multiple small intervals. Then we set a threshold value and determine whether each small interval belongs to the passband or the forbidden band. The number 1 is used here to indicate the passband and the number 0 to indicate the stopband. So that the second harmonic's passband and stopband characteristics can be represented by a simple one-dimensional array consisting of 1 and 0.

In this paper, we use CNNs and GRNNs to construct mapping relations between second harmonic band features and material parameters. And we also compare the performance of both neural networks.

A. THE CNN'S PRINCIPLE AND BASIC STRUCTURE

The Convolutional Neural Network (CNN) is a neural network model commonly used in areas such as image recognition, speech recognition, and natural language processing. In contrast to an image, the transmission curve is a one-dimensional signal. If the transmission curve image is directly used as input for training, the useless information will be greatly increased, which is not conducive to the prediction of metamaterials by the neural network. So we propose a one-dimensional neural network. The convolution kernel of the one-dimensional CNN is always moving in one dimensional direction. The related algorithms have a wide range of applications in speech recognition and fault detection. As shown in Fig. 3, it has a basic structure including the convolutional layer, the pooling layer, and the fully connected layer. The convolutional layer is the core part of CNN, which performs convolutional operations on the input signal to extract features for data identification. The pooling layer reduces the dimensionality of the feature map and reduces the computation, while also retaining the most important features. The fully connected layer is the last part of the neural network, which realizes the classification or prediction of the input by connecting the extracted features to the output layer.

In our work, the hidden layer consists of multiple fully connected layers. The deeper the hidden layer is, the better the ability to learn data features. The fully connected layer consists of multiple neurons, each consisting of an input,
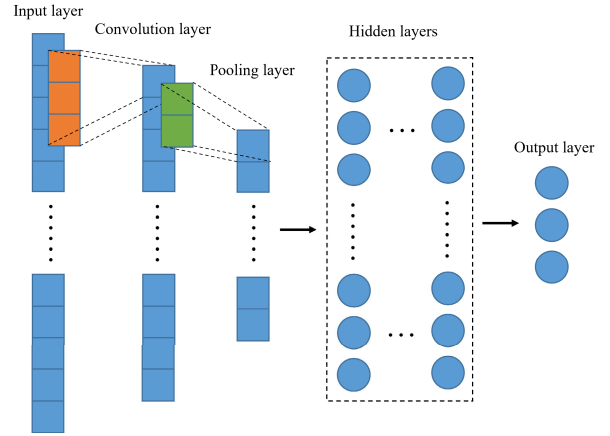
a weight, a bias, and an activation function. The output of each neuron is defined as:

$$y_o = g\left(wx + b\right). \tag{13}$$

Here x is the input, w is the weight, b is the bias, g is the activation function, and yo is the output of the neuron. The activation function we choose is the Relu function, which is commonly used as the activation function for CNNs due to its advantages of no gradient disappearance problem and faster training [27]. The Relu function is defined as:

$$g(x) = max(0, x). \tag{14}$$

The mean square error (MSE) function has been used a lot for high-precision estimation of finite sample posterior probabilities of neural networks, so we use the MSE function as the cost function, which is defined as:

$$L = \frac{1}{m} \sum \left(y_t - y_p\right)^2. \tag{15}$$

Here m is the number of sample sets in the training set, y_t is the target output (in this paper, the material parameters), and y_p is the output of the CNN in training. The training process of the CNN in this paper is carried out by the Adam gradient descent optimization algorithm [28], and a satisfactory neural network can be obtained by optimizing the cost function and adjusting the weights and biases so that it can predict the output more accurately.

The model graph of CNN is shown in Fig. 3.

B. THE GRNN'S PRINCIPLE AND BASIC STRUCTURE

General Regression Neural Network (GRNN) is a feedforward neural network, which is a modified form of Radial Basis Function Neural Network (RBF-NN), mainly composed of four layers: input layer, pattern layer, summation layer and output layer, as shown in Fig. 4. The input layer accepts the information from the external input, passes the information to the pattern layer, which processes the information by nonlinear mapping, then passes the processed result

to the summation layer, and finally the output layer performs the final calculation.

The most important feature of GRNN is that its pattern layer uses radial basis functions as activation functions. The radial basis is a type of local basis function that uses the distance between the input and the output of the pattern layer as the main reference factor for the function value. Common radial basis functions include the Gaussian function, polynomial function, etc. By adjusting the parameters of the radial basis function, the neural network can be adapted to different types of data. The radial basis function used in this paper is the Gaussian function, defined as:

$$g\left(r_i\right) = \exp\left(-\frac{\|r_i\|}{2\sigma^2}\right). \tag{16}$$

Here r_i represents the distance between the input sample and the learning sample of the ith pattern layer neuron and σ is the smoothing factor.

In GRNN, the number of neurons in the pattern layer is equal to the number of input samples, and the arithmetic sum and weighted sum of the summation layer are used to calculate the neural network prediction output. In contrast to the backpropagation algorithm, the weights of GRNN do not require iterative training, and their pattern layer weights are determined directly from the training samples. Then we can optimize the smoothing factor to obtain output results with excellent performance. Since GRNN usually have a simpler structure with fewer layers and parameters. The GRNN algorithm computes the weights and updates the parameters faster, leading to quicker train speed. Its output layer outputs as follows:

$$\mathcal{Y}_p = \frac{\sum_{i=1}^m w_i g\left(r_i\right)}{\sum_{i=1}^m g\left(r_i\right)}. \tag{17}$$

Here w_i is the weighting coefficient and y_p is the output of the GRNN. The GRNN neural network which can handle nonlinear problems, has strong adaptability and generalization ability and has a wide range of applications in curve fitting problems.

The model graph of GRNN is shown in Fig. 4.

C. NEURAL NETWORK-BASED INVERSE DESIGN PROCEDURE

After building the neural network, the model is trained using data from the training set, and then the model's generalizability is evaluated using the testing set. We evaluate the prediction accuracy of the model by calculating the root mean square error (RMSE) function of the target and predicted values. For the lower the RMSE value, the higher the prediction accuracy. RMSE is defined as:

$$RMSE = \sqrt{\frac{\sum_{i=1}^n \left(y_t - y_p\right)^2}{n}}. \tag{18}$$

Here y_t is the target value of material parameters, y_p is the predicted value of material parameters, and n is the number of output material parameters.
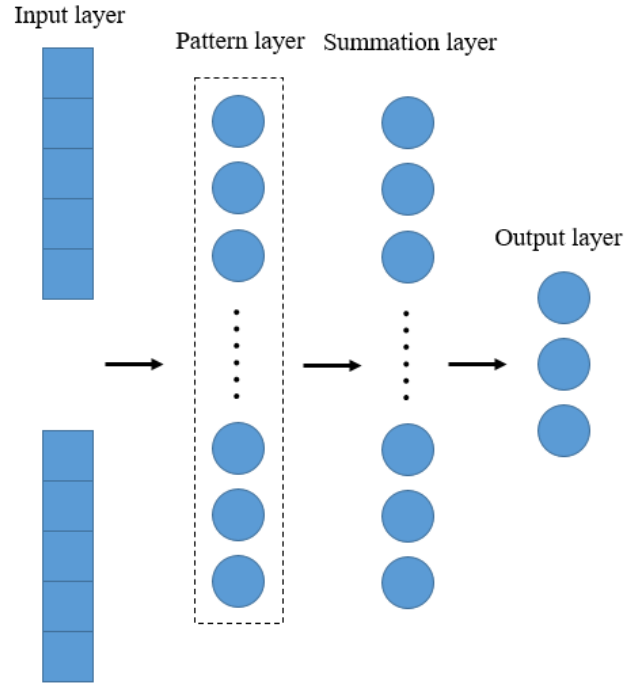

FIGURE 4. GRNN model graph.

In addition, because directly putting the transmission curves into the neural network processing will add a lot of redundant invalid information, and it is also not favorable to use the trained neural network for the prediction of phononic crystals. In order to better obtain the characteristics of the second harmonic transmission curve, we identify the transmission curves' stopband or passbands with 0 and 1, respectively. At first, the frequency range to be studied is set to 0-1 MHz, so that the first passband and the first forbidden band of each sample are completely covered. Then we use 1000 Hz as the unit frequency to divide the whole frequency range and set the threshold to determine the unit frequency is whether passband or stopband. This threshold is determined by both the transmission curve shape and the design goals. Based on the shape of the existing transmission curve, the threshold is set to -100 dB. The unit frequency interval of each sample falling in the passband or stopband is judged by the threshold value, identified by the numbers 1 and 0, respectively, and stored in a one-dimensional array as samples.

The inverse design process is shown in Fig. 5. First, the target transmission curve band features are represented by a 1×1000 one-dimensional array, which is then fed into a trained neural network. The network outputs the required material parameters, from which the predicted second harmonic transmission curve can be obtained.

IV. RESULTS AND DISCUSSIONS

We study the inverse design of a one-dimensional NPC for three cases. The parameters ζ, η are first considered; then the parameters ζ, η, $\overline{K}$ are considered; and finally four parameters ζ, η, $\overline{K}$ and Λ are considered.
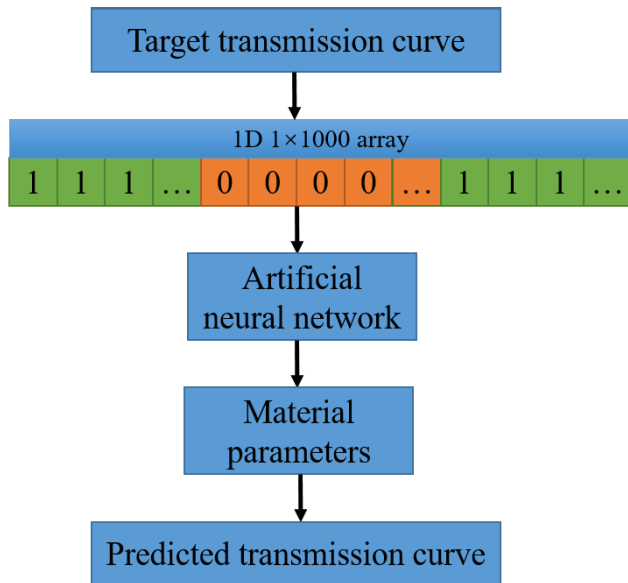
FIGURE 5. The NPC's inverse design flow graph.

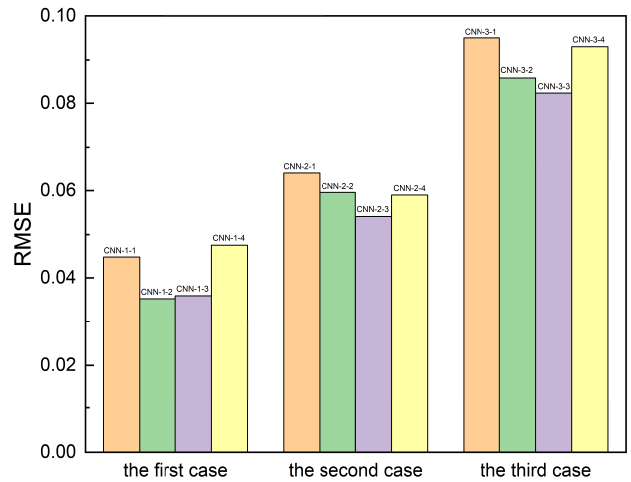FIGURE 6. The RMSE of the testing set for different CNNs.
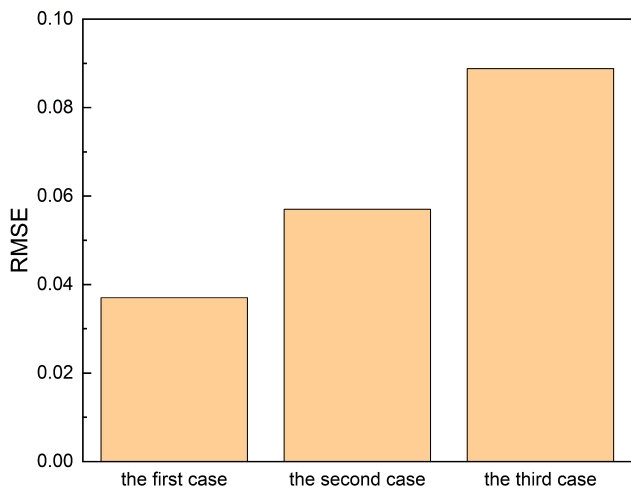
FIGURE 7. The RMSE of the testing set for different GRNNs.

A. CNN-BASED INVERSE DESIGN AND ANALYSIS

Different CNN neural network structures are selected for the three cases, and the RMSE is compared to determine the optimal structure of the CNN.

For the first case (two-parameter), the following four different CNN structures are compared.

CNN-1-1: 1000 - convolutional layer - pooling layer -500-200-100-50-2

CNN-1-2: 1000 - convolutional layer - pooling layer-500-200-100-50-50-2

CNN-1-3: 1000 - convolutional layer - pooling layer-500-200-100-50-50-50-2

CNN-1-4: 1000 - convolutional layer - pooling layer-500-200-100-50-50-50-50-2

For the second case (three parameters), the following four different CNN structures are compared.

CNN-2-1: 1000 - convolutional layer - pooling layer-800-400-200-100-3

CNN-2-2: 1000 - convolutional layer - pooling layer-800-400-200-100-100-3

CNN-2-3: 1000 - convolutional layer - pooling layer-800-400-200-100-100-100-3

CNN-2-4: 1000 - convolutional layer - pooling layer-800-400-200-100-100-100-100-3

For the third case (four parameters), the following four different CNN structures are compared.

CNN-3-1: 1000 - convolutional layer - pooling layer-1000-800-400-200-100-4

CNN-3-2: 1000 - convolutional layer - pooling layer-1000-800-400-200-100-100-4

CNN-3-3: 1000 - convolutional layer - pooling layer-1000-800-400-200-100-100-100-4

CNN-3-4: 1000 - convolutional layer - pooling layer-1000-800-400-200-100-100-100-100-4

Here, "1000" is the number of dimensions of the input layer samples, and "2", "3", "4" are the number of neurons in the output layer. The convolutional layer is a one-dimensional convolutional kernel to extract features from the input data, and the size of the convolutional kernel is 3. The pooling layer adopts the maximum pooling strategy, and the size of the convolutional kernel is 2. The rest is the number of hidden layer neurons. Too many neurons may lead to overfitting, while too few neurons may lead to underfitting. Therefore, the method of verifying the performance of the testing set is used to determine the appropriate number of neurons. The RMSE of the testing set with different CNN structures for the three cases is given in Fig. 6. It is shown that for the first case, the prediction error of CNN-1-2 is smaller; for the second case, the prediction error of CNN-2-3 structure is smaller; for the third case, the prediction error of CNN-3-3 structure is smaller.

B. GRNN-BASED INVERSE DESIGN AND ANALYSIS

For GRNN, we set the number of neurons in the pattern layer equal to the number of input samples. For the first
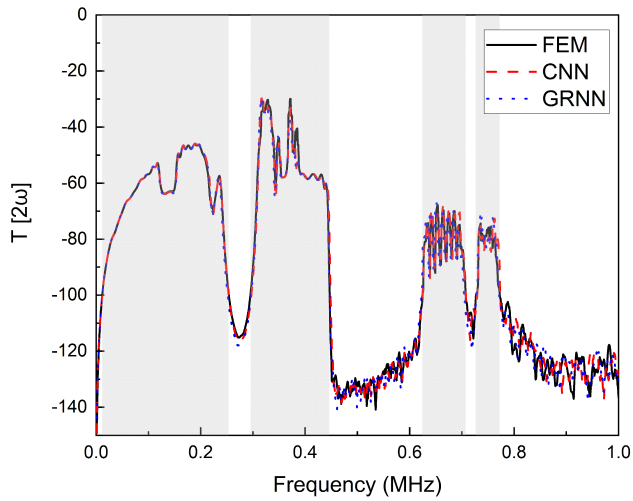
(a)
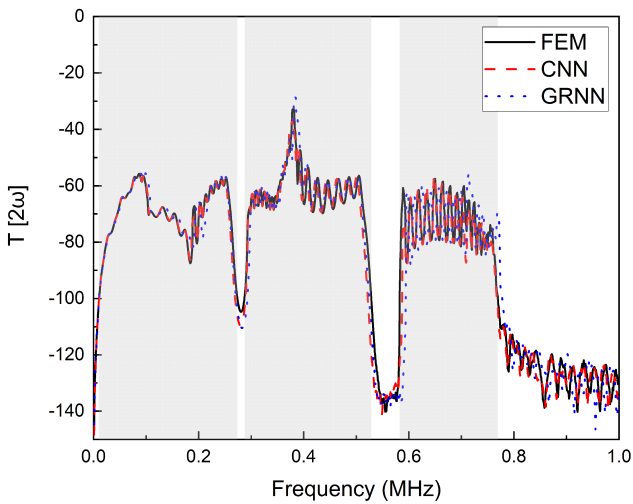
(b)

FIGURE 8. The target and predicted second harmonic transmission curve of the testing set A(FEM indicates the target transmission curve, CNN and GRNN indicate the transmission curve predicted by CNN and GRNN, respectively).

case, the GRNN structure is set to be GRNN-1: 1000-80-Summation layer-1; for the second case, the GRNN structure is set to be GRNN-2: 1000-800-Summation layer-2; for the third case, the GRNN structure is set to be GRNN-3: 1000-8000-Summation layer-3.

The GRNNs' RMSE of the testing set for the three cases are given in Fig. 7. It can be seen that the prediction error stays at a better scale for all three cases.

C. COMPARATIVE ANALYSIS OF CNN AND GRNN

Here, the NPC parameters are predicted for three cases and the target and predicted transmission curves of the second harmonic are compared to verify the neural network performance. The structures of CNN in the three cases are CNN-1-2,CNN-2-3,CNN-3-3, and the structures of GRNN are GRNN-1, GRNN-2, and GRNN-3 respectively.
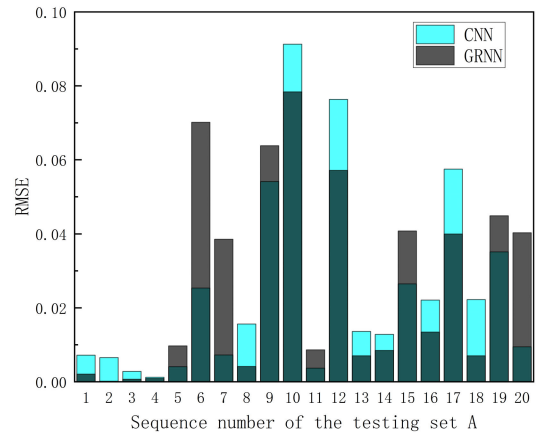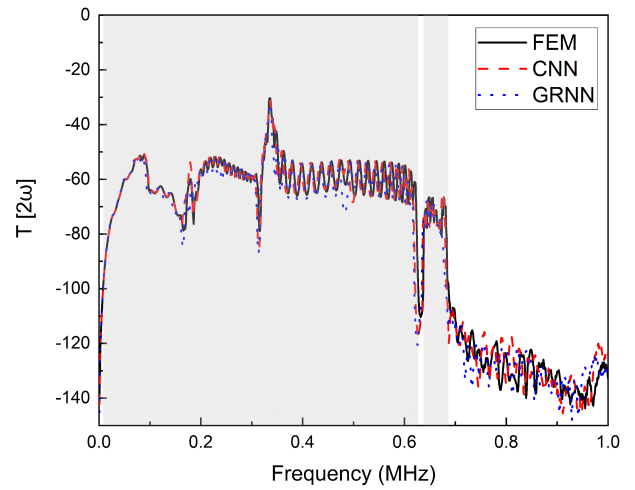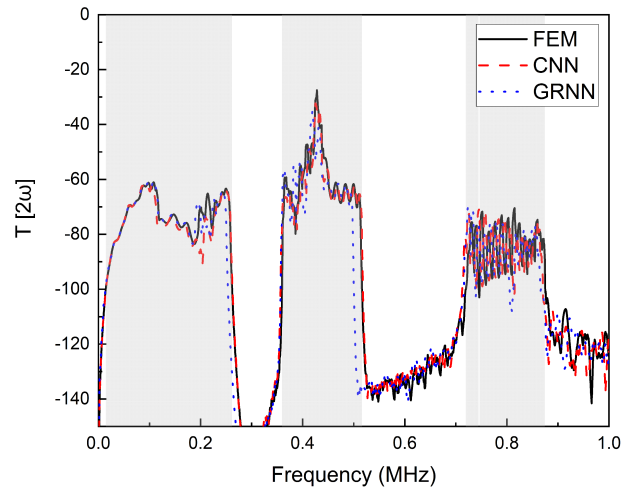

FIGURE 9. Prediction accuracy of CNN and GRNN for the testing set A.

(a)

(b)

FIGURE 10. The target and predicted second harmonic transmission curve of the testing set B.

In the first case, the density ratio and sound velocity ratio of NPC are predicted. The data set consists of the training set
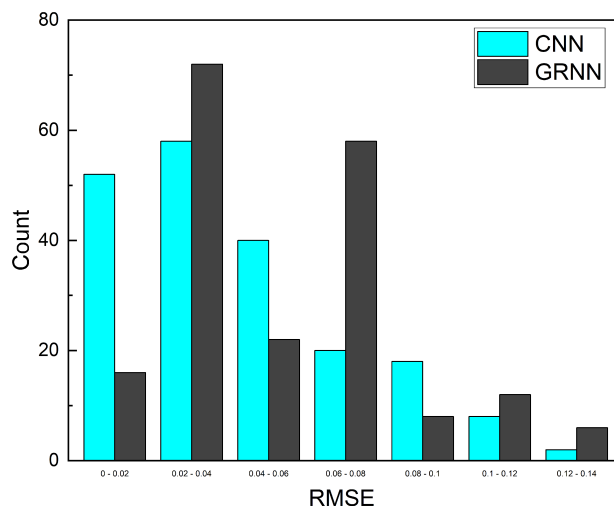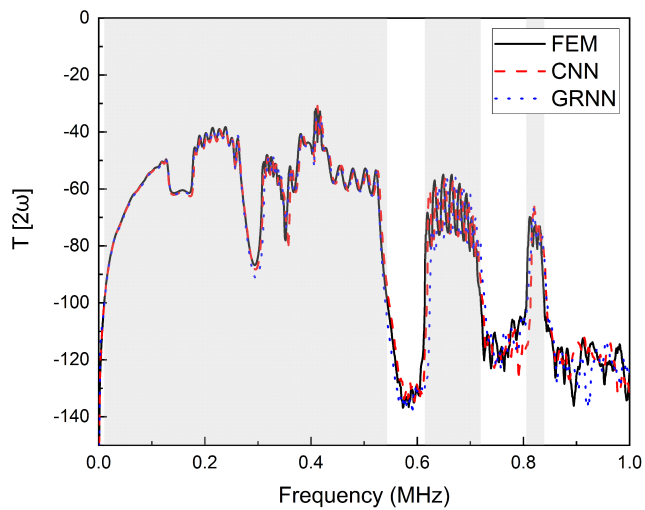
FIGURE 11. The error statistics of CNN and GRNN for the testing set B.

TABLE 3. Comparison of CNN and GRNN. Training time refers to the time required to train the neural network, and computation time refers to the time required to inversely design the NPC parameters by the neural network.
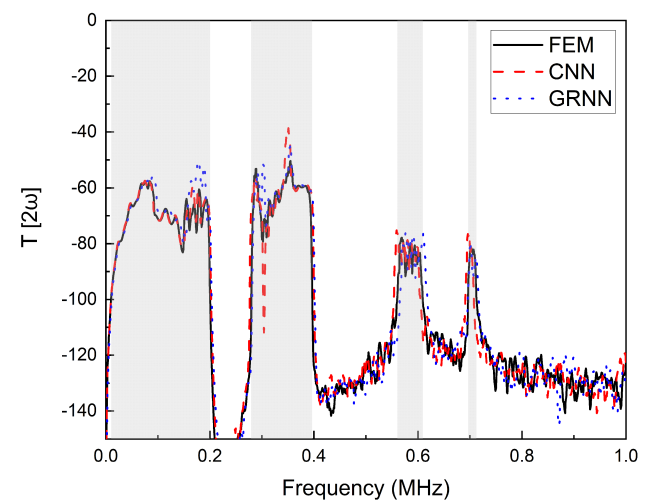
Cases considered	Method	Training time(s)	Calculation time(s)	RMSE
Case1: two parameter	CNN	116	0.02	0.035
	GRNN	0.06	0.01	0.037
Case2: three parameter	CNN	346	0.03	0.054
	GRNN	0.22	0.02	0.057
Case3: four parameter	CNN	628	0.05	0.082
	GRNN	0.82	0.09	0.089

(a)

(b)

FIGURE 12. The target and predicted second harmonic transmission curve of the testing set C.

A and the testing set A. The second harmonic transmission curves that are calculated by the physical parameters predicted by the neural network for the testing set A are shown in Fig. 8 (due to the space limitation, only two sets of predictions for the testing set A, B, and C are shown as examples). The gray area in the figure indicates the band where the input target transmission curve is ''1'', and the white area indicates the band where the input target transmission curve is ''0''. FEM denotes the target transmission curve, and CNN and GRNN denote the transmission curves calculated by CNN and GRNN prediction, respectively. The prediction accuracy is shown in Fig. 9. Both neural networks show good performance in predicting the transmission curves, where the CNN performs better, but the GRNN has a much shorter training time.

In the second case, we inversely design the NPC's three parameters: density ratio, sound velocity ratio, and normalized interface linear stiffness. The data set consists of the training set B and the testing set B. Here the two sets of

predictions for the testing set B are shown as examples, in Fig. 10. It can be seen from the figure that for the three-parameter prediction, both neural networks also give satisfactory results. The error statistics for the testing set B's predicted results is shown in Fig. 11. The prediction error mostly stays in a small range, and the prediction error of CNN is smaller than that of GRNN.

In the third case, we inverse design the NPC's four parameters: material thickness ratio, density ratio, sound velocity ratio, and normalized interface linear stiffness. The data set consists of the training set C and the testing set C. Fig. 12 shows the two sets of prediction results for the testing set C. The error statistics of the testing set C are shown in Fig. 13. It can be seen that the prediction results of both neural networks are still better, and the prediction error of CNN is still smaller than that of GRNN.

The comparison of CNN and GRNN is shown in Table 3. It is shown that the computational time required to predict
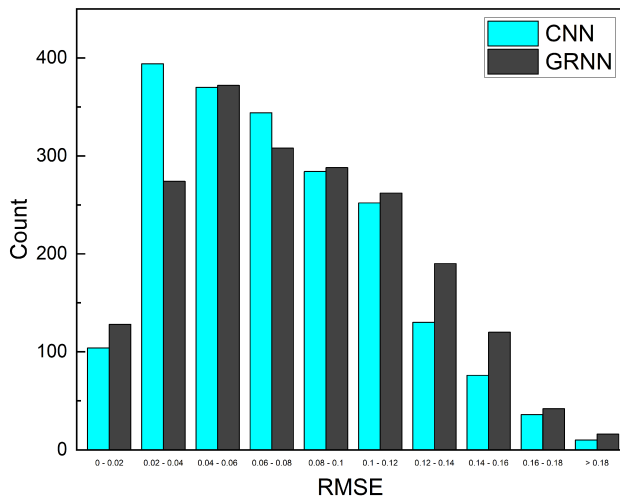
FIGURE 13. The error statistics of CNN and GRNN for the testing set C.

by neural network is extremely short, and the computational speed is much better than the traditional method which is with continuous trial and error. In addition, the neural network prediction accuracy is excellent. For the three cases of prediction, CNN is better than GRNN in terms of prediction accuracy, while GRNN is better than CNN in terms of training time and model simplicity. We can choose different neural network models according to the actual situation.

V. CONCLUSION

In this paper, both CNN and GRNN models are trained and an inverse design method for one-dimensional NPC is proposed. The method uses the band structure of target transmission curve as the input to the neural network, and the network will output the corresponding NPC material parameters. The designed material parameters include density ratio, sound velocity ratio, interface stiffness and thickness ratio. For all three cases of design, CNN and GRNN exhibit satisfactory performance. In particular, CNNs exhibit more precise prediction accuracy, while GRNNs have unique advantages in terms of training speed and model simplicity. Compared with traditional algorithms, the neural network construction requires a large number of samples for training, and although the method requires some time and computational resources, the process can be done in parallel and at once. At the same time, the method differs from the traditional methods relying on analytical theory and parametric analysis, providing new ideas for the inverse design of metamaterials.

This paper demonstrates the feasibility and superiority of neural network-based inverse design for NPCs. In fact, two and three dimensional metamaterials will be more complex in design and computation, consuming more time and computational resources. Therefore, it will be more meaningful to apply neural networks to two or three dimensional metamaterial design. The present work provides a useful foundation for future related research.

REFERENCES

[1] T. Ma, X. Su, H. Dong, Y. Wang, and C. Zhang, "Review of bandgap characteristics and acousto-optical coupling in phoxonic crystals," *Chin. J. Theor. Appl. Mech.*, vol. 49, no. 4, pp. 743–757, 2017, doi: 10.6052/0459-1879-17-130.

[2] J. Cabaret, V. Tournat, and P. Béquin, "Amplitude-dependent phononic processes in a diatomic granular chain in the weakly nonlinear regime," *Phys. Rev. E, Stat. Phys. Plasmas Fluids Relat. Interdiscip. Top.*, vol. 86, no. 4, Oct. 2012, Art. no. 041305, doi: 10.1103/PhysRevE.86.041305.

[3] T. J. Delph, G. Herrmann, and R. K. Kaul, "Harmonic wave propagation in a periodically layered, infinite elastic body: Antiplane strain," *J. Appl. Mech.*, vol. 45, no. 2, pp. 343–349, Jun. 1978, doi: 10.1115/1.3424299.

[4] S. Biwa, S. Nakajima, and N. Ohno, "On the acoustic nonlinearity of solid-solid contact with pressure-dependent interface stiffness," *J. Appl. Mech.*, vol. 71, no. 4, pp. 508–515, Jul. 2004, doi: 10.1115/1.1767169.

[5] Z. N. Li, Y. Z. Wang, and Y. S. Wang, "Tunable mechanical diode of nonlinear elastic metamaterials induced by imperfect interface," *Proc. Roy. Soc. A, Math., Phys. Eng. Sci.*, vol. 477, no. 2245, 2021, Art. no. 20200357, doi: 10.1098/rspa.2020.0357.

[6] Y. Ishii and S. Biwa, "Acoustic harmonic generation in a multilayered structure with nonlinear interfaces," in *Proc. AIP Conf.*, 2012, pp. 223–226, doi: 10.1063/1.4749336.

[7] Y. Ishii and T. Adachi, "Analysis of acoustic second-harmonic generation in alternating multilayered structure with closed defect at interlayer interface," *J. Soc. Mater. Sci., Jpn.*, vol. 68, no. 4, pp. 358–365, 2019, doi: 10.2472/jsms.68.358.

[8] Y.-F. Wang, Y.-Z. Wang, B. Wu, W. Chen, and Y.-S. Wang, "Tunable and active phononic crystals and metamaterials," *Appl. Mech. Rev.*, vol. 72, no. 4, Jul. 2020, doi: 10.1115/1.4046222.

[9] J. Y. Liu, H. B. Guo, and T. Wang, "A review of acoustic metamaterials and phononic crystals," *Crystals*, vol. 10, no. 4, p. 305, 2020, doi: 10.3390/cryst10040305.

[10] C. X. Liu and G. L. Yu, "Deep learning for the design of phononic crystals and elastic metamaterials," *J. Comput. Design Eng.*, vol. 10, no. 2, pp. 602–614, 2023, doi: 10.1093/jcde/qwad013.

[11] Y. Jin et al., "Intelligent on-demand design of phononic metamaterials," *Nanophotonics*, vol. 11, no. 3, pp. 439–460, 2022, doi: 10.1515/nanoph-2021-0639.

[12] Y. Li, D. Chen, X. Li, and W. Wang, "Vibration transmission characteristic prediction and structure inverse design of acoustic metamaterial beams based on deep learning," *J. Vibrat. Control*, Jan. 2023, Art. no. 107754632311514, doi: 10.1177/10775463231151462.

[13] Y. X. Jing, H. C. Chu, B. Huang, J. Luo, W. Wang, and Y. Lai, "A deep neural network for general scattering matrix," *Nanophotonics*, vol. 12, no. 13, p. 0770, 2023, doi: 10.1515/nanoph-2022-0770.

[14] J. Peurifoy et al., "Nanophotonic particle simulation and inverse design using artificial neural networks," *Sci. Adv.*, vol. 4, no. 6, p. 4206, 2018, doi: 10.1126/sciadv.aar4206.

[15] D. Finol, Y. Lu, V. Mahadevan, and A. Srivastava, "Deep convolutional neural networks for eigenvalue problems in mechanics," *Numer. Methods Eng.*, vol. 118, no. 5, pp. 258–275, 2018, doi: 10.1002/nme.6012.

[16] W. W. Ahmed, M. Farhat, X. Zhang, and Y. Wu, "Deterministic and probabilistic deep learning models for inverse design of broadband acoustic cloak," *Phys. Rev. Res.*, vol. 3, no. 1, Feb. 2021, Art. no. 013142, doi: 10.1103/PhysRevResearch.3.013142.

[17] T. W. Liu, C. T. Chan, and R. T. Wu, "Deep-learning-based acoustic metamaterial design for attenuating structure-borne noise in auditory frequency bands," *Materials*, vol. 16, no. 5, p. 1879, 2023, doi: 10.3390/ma16051879.

[18] C. Gurbuz, F. Kronowetter, C. Dietz, M. Eser, J. Schmid, and S. Marburg, "Generative adversarial networks for the design of acoustic metamaterials," *J. Acoust. Soc. Amer.*, vol. 149, no. 2, pp. 1162–1174, Feb. 2021, doi: 10.1121/10.0003501.

[19] C.-X. Liu, G.-L. Yu, and G.-Y. Zhao, "Neural networks for inverse design of phononic crystals," *AIP Adv.*, vol. 9, no. 8, Aug. 2019, doi: 10.1063/1.5114643.

[20] L. He, H. Guo, Y. Jin, X. Zhuang, T. Rabczuk, and Y. Li, "Machine-learning-driven on-demand design of phononic beams," *Sci. China Phys., Mech. Astron.*, vol. 65, no. 1, p. 1787, Jan. 2022, doi: 10.1007/s11433-021-1787-x.

[21] I. Grinberg and K. H. Matlack, "Nonlinear elastic wave propagation in a phononic material with periodic solid-solid contact interface," *Wave Motion*, vol. 93, Mar. 2020, Art. no. 102466, doi: 10.1016/j.wavemoti.2019.102466.

[22] S. Liang, J. Liu, Y. Lai, and X. Liu, "Nonlinear wave propagation in acoustic metamaterials with bilinear nonlinearity," *Chin. Phys. B*, vol. 32, no. 4, Apr. 2023, Art. no. 044301, doi: 10.1088/1674-1056/ac9783.

[23] Z. Chen, W. Zhou, and C. W. Lim, "Active control for acoustic wave propagation in nonlinear diatomic acoustic metamaterials," *Int. J. Non-Linear Mech.*, vol. 125, Oct. 2020, Art. no. 103535, doi: 10.1016/j.ijnonlinmec.2020.103535.

[24] M. Song and W. Zhu, "Elastic wave propagation in strongly nonlinear lattices and its active control," *J. Appl. Mech.*, vol. 88, no. 7, Jul. 2021, Art. no. 071003, doi: 10.1115/1.4050394.

[25] Y.-Z. Wang and Y.-S. Wang, "Active control of elastic wave propagation in nonlinear phononic crystals consisting of diatomic lattice chain," *Wave Motion*, vol. 78, pp. 1–8, Apr. 2018, doi: 10.1016/j.wavemoti.2017.12.009.

[26] J. M. Manimala and C. T. Sun, "Numerical investigation of amplitude-dependent dynamic response in acoustic metamaterials with nonlinear oscillators," *J. Acoust. Soc. Amer.*, vol. 139, no. 6, pp. 3365–3372, Jun. 2016, doi: 10.1121/1.4949543.

[27] Z. S. Zheng et al., "Deep learning model for Typhon grade classification based on improved activation function," *Comput. Sci.*, vol. 45, no. 12, pp. 177–181, 2018.

[28] D. P. Kingma and J. Ba, "Adam: A method for stochastic optimization," 2014, *arXiv:1412.6980*.

YUANYUAN LI received the B.S. degree in measurement and control technology and instruments and the M.S. degree in precision instruments and machinery from Nanchang Hangkong University, Nanchang, China, in 2017 and 2020, respectively. She is currently pursuing the Ph.D. degree in acoustics with Nanjing University, Nanjing, China. Her research interests include ultrasonic nondestructive testing and acoustic metamaterials.

YUN LAI received the Ph.D. degree from The Hong Kong University of Science and Technology (HKUST), Hong Kong, in 2005. He was a Research Associate with the Department of Physics, HKUST. In 2011, he became a Professor with Soochow University. In 2018, he joined the School of Physics, Nanjing University, as a Professor. His research interests include optical, electromagnetic and acoustic metamaterials, metasurfaces, nanophotonics, plasmonics, photonic, and phononic crystals. He has published more than 120 papers on SCI journals including, *Science*, *Nature Materials*, *Physical Review Letters/X*, *Nature Communications*, and *Science Advances*, with the total citation number exceeding 6000. He has pioneered some key concepts, such as illusion optics, zero-index materials, transparent matte surfaces, anomalous Brewster effect, and zero-spacing waveguide systems. He is currently the Co-Editor of *EPL* and an Editorial Board Member of *Optical and Quantum Electronics*.

KUNQI HUANG received the B.S. degree in marine technology from Xiamen University, Xiamen, China, in 2021. He is currently pursuing the M.S. degree in acoustics with Nanjing University, Nanjing, China. His research interests include ultrasonic nondestructive testing and acoustic metamaterials.

XIAOZHOU LIU received the Ph.D. degree in acoustics from Nanjing University, Nanjing, China, in 1999. Since 2007, he has been a Professor with Nanjing University. He was a Visiting Scholar with Pennsylvania State University, University Park, PA, USA, in 2009. Over the past 30 years, he has conducted both theoretical and experimental research on acoustics. He has authored over 160 research articles. His current research interests include nonlinear acoustics, medical ultrasound, and ultrasonic nondestructive testing.

• • •